Article

Redox-Active Organometallics: Magnetic and Electronic Couplings through Carbon#Silicon Hybrid Molecular Connectors

Paul Hamon, Frederic Justaud, Olivier Cador, Philippe Hapiot, Ste#phane Rigaut, Loi#c Toupet, Lahce#ne Ouahab, Harald Stueger, Jean-Rene# Hamon, and Claude Lapinte

J. Am. Chem. Soc., **2008**, 130 (51), 17372-17383 • DOI: 10.1021/ja804608z • Publication Date (Web): 21 November 2008

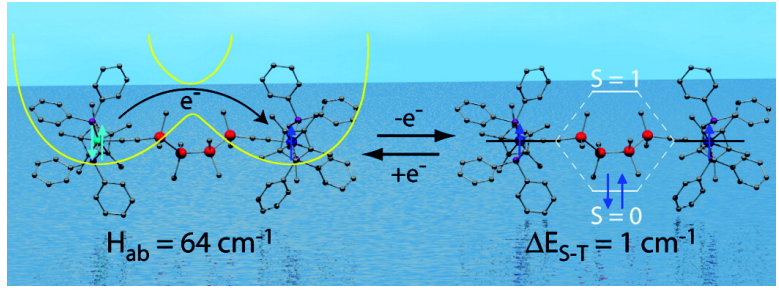

More About This Article

Additional resources and features associated with this article are available within the HTML version:

- Supporting Information
- Access to high resolution figures
- Links to articles and content related to this article
- Copyright permission to reproduce figures and/or text from this article

View the Full Text HTML

J|A|C|S
ARTICLES

Published on Web 11/21/2008

Redox-Active Organometallics: Magnetic and Electronic Couplings through Carbon−Silicon Hybrid Molecular Connectors

Paul Hamon,[†] Frederic Justaud,[†] Olivier Cador,[†] Philippe Hapiot,[†] Stéphane Rigaut,[†] Loïc Toupet,[‡] Lahcène Ouahab,[†] Harald Stueger,*[,§] Jean-René Hamon,*[,†] and Claude Lapinte*[,†]

UMR CNRS 6226 Sciences Chimiques de Rennes and UMR CNRS 6251 Institut de Physique de Rennes, Université de Rennes 1, Campus de Beaulieu, F-35042 Rennes, France, and Institut für Anorganische Chemie, Technische Universität Graz, Stremayrgasse 16, A-8010 Graz, Austria

Received June 17, 2008; E-mail: harald.stueger@tugraz.at; jrhamon@univ-rennes1.fr; lapinte@univ-rennes1.fr

Abstract: Treatment of the triflate complex Cp*(dppe)FeOTf [**12**; Cp* = η^5-$C_5(CH_3)_5$, dppe = 1,2-bis(diphenylphosphino)ethane, OTf = CF_3SO_3] with an excess of HC≡C−$(Si(CH_3)_2)_x$−C≡CH ($x = 2-4$) in diethyl ether provides the binuclear bis(vinylidene) derivatives [Cp*(dppe)Fe═C═CH$(Si(CH_3)_2)_x$CH═C═Fe(dppe)Cp*][OTf]$_2$ ($x = 2$, **13**; $x = 3$, **14**; $x = 4$, **15**), which were isolated as ochre solids and rapidly characterized by FT-IR, ^{1}H, ^{31}P, and ^{13}C NMR spectroscopies. The complexes **13**−**15** were reacted with potassium *tert*-butoxide to afford the bis(alkynediyl) complexes [Cp*(dppe)Fe−C≡C$(Si(CH_3)_2)_x$C≡C−Fe(dppe)Cp*] ($x = 2$, **1**; $x = 3$, **2**; $x = 4$, **3**), which were isolated as orange powders in yields ranging from 76 to 91%. The IR, cyclic voltammetry, and UV−vis data obtained for **1**−**3** and the X-ray crystal structures determined for **1** and **3** reveal the importance of the $\sigma-\pi$ conjugation (hyperconjugation) between the Si−Si σ bond and the adjacent C≡C π-symmetric orbitals in the description of the electronic structure of the ground state of these complexes. When reacted at low temperature with 2 equiv of $[(C_5H_5)_2Fe]X$ or AgX [X = BPh_4, $B(3,5\text{-}(CF_3)_2C_6H_3)_4$)], compounds **1**−**3** provide **1**$[X]_2$, **2**$[X]_2$, and **3**$[X]_2$, which can be isolated and stored below −20 °C. EPR spectroscopy and magnetization measurements established that the superexchange interaction propagates through the Si−Si bonds ($J = -0.97(2)$ cm^{-1} for **3**$[X]_2$). UV−vis−near-IR spectra were obtained with an optically transparent thin-layer electrosynthetic (OTTLE) cell for **1**−**3**$[OTf]_n$ ($n = 0-2$). A band with a maximum that increases from 6400 cm^{-1} (**1**[OTf]) to 8500 cm^{-1} (**3**[OTf]) observed for the mixed-valence species was ascribed to intervalence charge transfer evidencing photodriven electron transfer through the carbon−silicon hybrid connectors with H_{ab} parameters ranging from 64 to 285 cm^{-1}.

Introduction

The molecular sciences of the transition metals have potential applications in the new fascinating field of molecular electronics.[1−3] This hope is based inter alia on the fact that the oxidation states of transition metals can be varied to a great extent and thus that many electron- and charge-transfer processes can result.[4,5] By suitable molecular engineering, it should become possible to assemble and tune molecular devices including transition metals and organize their interface with the macroscopic world.[6] The interplay between light, electron transfer, and magneto-optic properties will then provide efficient and precise molecular sensors for the various needs of future technology. In this context, metal-containing long-chain conjugated systems have emerged as an important category of materials expected to have significantly different properties from organic conjugated oligomers.[7−12] Alkynyl bridges, with the linear geometry of the C≡C unit, offer the advantages of possessing low-lying, unoccupied π* orbitals and high polarizability of the π-electron clouds, which provide an opportunity for the observation of nonlinear optical, conducting, and liquid-crystalline properties

[†] Sciences Chimiques de Rennes.
[‡] Institut de Physique de Rennes.
[§] Institut für Anorganische Chemie.

(1) Robertson, N.; McGowan, G. A. *Chem. Soc. Rev.* **2003**, *32*, 96–103.
(2) Caroll, R. L.; Gorman, C. B. *Angew. Chem., Int. Ed.* **2002**, *41*, 4379–4400.
(3) Tour, J. M. *Acc. Chem. Res.* **2000**, *33*, 791–803.
(4) Barbara, P. F.; Meyer, T. J.; Ratner, M. A. *J. Phys. Chem.* **1996**, *100*, 13148–13168.
(5) Astruc, D. *Electron Transfer and Radical Processes in Transition-Metal Chemistry*; VCH: New York, 1995.
(6) Kim, B.; Beebe, J. M.; Olivier, C.; Rigaut, S.; Touchard, D.; Kushmerick, J. G.; Zhu, X.-Y.; Frisbie, C. D. *J. Phys. Chem. C* **2007**, *111*, 7521–7526.
(7) Samoc, M.; Gauthier, N.; Cifuentes, M. P.; Paul, F.; Lapinte, C.; Humphrey, M. G. *Angew. Chem., Int. Ed.* **2006**, *45*, 7376–7379.
(8) Schwab, P. F. H.; Levin, M. D.; Michl, J. *Chem. Rev.* **2005**, *105*, 1197–1279.
(9) Schwab, P. F. H.; Levin, M. D.; Michl, J. *Chem. Rev.* **1999**, *99*, 1863–1933.
(10) Fillaut, J.-L.; Perruchon, J.; Blanchard, P.; Roncali, J.; Gohlen, S.; Allain, M.; Migalska-Zalas, A.; Kityk, I. V.; Sahraoui, B. *Organometallics* **2005**, *24*, 687–695.
(11) Szafert, S.; Gladysz, J. A. *Chem. Rev.* **2003**, *103*, 4175–4205.
(12) Wong, K. M.-C.; Lam, S. C.-F.; Ko, C.-C.; Zhu, N.; Yam, V. W.-W.; Roué, S.; Lapinte, C.; Fathallah, S.; Costuas, K.; Kahlal, S.; Halet, J.-F. *Inorg. Chem.* **2003**, *42*, 7086–7097.

10.1021/ja804608z CCC: $40.75

as well as their potential to act as a molecular connectors for magnetic and electronic communication.[13−25]

In previous papers, the synthesis and physical properties of bis(iron) molecules having the general formula $[Cp^*(dppe)Fe-C\equiv C-X-C\equiv C-Fe(dppe)Cp^*][PF_6]_n$ [X = none,[14,24] $-C\equiv C-C\equiv C-$,[15,26] 1,4-C_6H_4,[13,27] 9,10-$C_{14}H_8$,[19] 1,3-C_6H_4 (**6**),[28] 2,5-C_4H_2S;[29] $n = 0, 1, 2$; $Cp^* = \eta^5$-$C_5(CH_3)_5$, dppe = 1,2-bis(diphenylphosphino)ethane] were reported. All of these compounds were isolated as stable Fe(II)−Fe(II), Fe(II)−Fe(III), and Fe(III)−Fe(III) derivatives, and the investigation of their spectroscopic and magnetic properties revealed electronic and magnetic coupling with various strength between the metal ends.[30−32] On the other hand, a redox family of compounds containing a saturated hydrocarbon fragment inserted into the carbon-rich bridge [X = $(CH_2)_x$, $x = 3$ (**4**), 4 (**5**); $n = 0, 1, 2$] was also prepared and studied.[33] In this case, cyclic voltammetry (CV) and IR, Mössbauer, EPR, and UV−vis spectra provided evidence for a weak through-bridge interaction between the iron sites. Near-IR (NIR) spectroscopy of the mixed-valence (MV) complexes clearly shows that through-bridge electron transfer occurs.[33]

On the other hand, the unique properties of silicon have given rise to the development of most existing electronic devices. Connecting the donor and acceptor groups by polysilane backbones is considered to be attractive because of the following features: (i) increased polarizability of silicon chains as compared with the carbon analogues, (ii) $\sigma-\pi$ interactions [σ(Si)−π(C)], and (iii) electron delocalization over the Si−Si bonds via σ conjugation.[34−40] Under certain circumstances, therefore, σ-(Si−Si)-bonded donor−bridge−acceptor compounds might be suitable candidates for the synthesis of materials having interesting properties of technological significance, such as nonlinear optical activity.[41−44]

The main aim of this paper is to report our investigations on new hybrid inorganic/organometallic molecules that incorporate silicon atoms into carbon-rich bridges between iron centers with d^5 and d^6 electronic configurations. Our efforts were focused on the synthesis of the three new compounds **1**−**3**, in which one, two, and three Si−Si bonds, respectively, were inserted into the carbon-rich bridge (see Chart 1), and on measurements of the physical properties of these complexes in three different oxidation states (compounds $\mathbf{1}^{n+}[X^-]_n-\mathbf{3}^{n+}[X^-]_n$, $n = 0, 1, 2$) and a comparison with the related silicon-free compounds $\mathbf{4}^{n+}[X^-]_n-\mathbf{6}^{n+}[X^-]_n$ in regard to their merit in terms of electronic and magnetic couplings.

Results and Discussion

1. Synthesis of 1, 2, and 3. Some of us previously reported that treatment of the terminal bis(alkyne) molecules $HC\equiv C-(CH_2)_x-C\equiv CH$ ($x = 3, 4$) with 2 equiv of Cp*(dppe)FeCl (**8**) in methanol in the presence of $NaBPh_4$ or KPF_6 provided the bis(vinylidene) complexes $[Cp^*(dppe)Fe{=}C{=}CH-(CH_2)_x-HC{=}C{=}Fe(dppe)Cp^*][X]_2$ [$x = 3$ (**4H$_2$**), 4 (**5H$_2$**), X = BPh_4, PF_6) in high yield (Scheme S1 in the Supporting Information).[33] In a similar approach, reactions between **8** and $HC\equiv C-(Si(CH_3)_2)_x-C\equiv CH$ ($x = 2-4$) led to the breaking of the C(sp)−Si bonds; thus, the mononuclear vinylidene $[Cp^*(dppe)Fe{=}C{=}CH_2][PF_6]$ (**9**) was isolated as the unique organoiron derivative,[14] while siloxanes **10** and **11** were formed through hydrolysis processes (see Scheme S1). To overcome this difficulty, an alternative approach starting from the known triflate complex Cp*(dppe)FeOTf (**12**, OTf = OSO_2CF_3), which dissociates in nonpolar solvents,[45] was envisaged.

Thus, **12** was reacted with an excess of $HC\equiv C-(Si(CH_3)_2)_x-C\equiv CH$ ($x = 2, 3, 4$) in diethyl ether, and the initially green suspension progressively turned yellow upon stirring overnight (Scheme 1). The solid materials were isolated by filtration and identified as the expected binuclear bis(vinylidene) derivatives $[Cp^*(dppe)Fe{=}C{=}CH(Si(CH_3)_2)_xCH{=}C{=}Fe(dppe)Cp^*][OTf]_2$ (**13**, $x = 2$; **14**, $x = 3$; **15**, $x = 4$). These complexes were apparently stable in the solid state but readily decomposed in solution to give rise to the mononuclear vinylidene **9**.[14] For this reason, compounds **13**−**15** were only partially characterized by FT-IR, ^{1}H, ^{31}P, and ^{13}C NMR

(13) Le Narvor, N.; Lapinte, C. *Organometallics* **1995**, *14*, 634–639.
(14) Le Narvor, N.; Toupet, L.; Lapinte, C. *J. Am. Chem. Soc.* **1995**, *117*, 7129–7138.
(15) Coat, F.; Paul, F.; Lapinte, C.; Toupet, L.; Costuas, K.; Halet, J.-F. *J. Organomet. Chem.* **2003**, *683*, 368–378.
(16) Weyland, T.; Ledoux, I.; Brasselet, S.; Zyss, J.; Lapinte, C. *Organometallics* **2000**, *19*, 5235–5237.
(17) Cifuentes, M. P.; Humphrey, M. G.; Morrall, J. P.; Samoc, M.; Paul, F.; Lapinte, C.; Roisnel, T. *Organometallics* **2005**, *24*, 4280–4288.
(18) Paul, F.; Costuas, K.; Ledoux, I.; Deveau, S.; Zyss, J.; Halet, J.-F.; Lapinte, C. *Organometallics* **2002**, *21*, 5229–5235.
(19) de Montigny, F.; Argouarch, G.; Costuas, K.; Halet, J.-F.; Roisnel, T.; Toupet, L.; Lapinte, C. *Organometallics* **2005**, *24*, 4558–4572.
(20) Qi, H.; Noll, B.; Snider, G. L.; Lu, Y.; Lent, S. S.; Felhner, T. P. *J. Am. Chem. Soc.* **2005**, *127*, 15218–15227.
(21) Blum, A. S.; Ren, T.; Parish, D. A.; Trammell, S. A.; Moore, M. H.; Kushmerick, J. G.; Xu, G. L.; Deschamps, J. R.; Polack, S. K.; Shashidar, R. *J. Am. Chem. Soc.* **2005**, *127*, 10010–10011.
(22) Xu, G. L.; Crutchley, R. J.; DeRosa, M. C.; Pan, Q.-J.; Zhang, H.-X.; Wang, X.; Ren, T. *J. Am. Chem. Soc.* **2005**, *127*, 13354–13363.
(23) Schull, T. L.; Kushmerick, J. G.; Patterson, C. H.; George, C.; Moore, M. H.; Pollack, S. K.; Shashidar, R. *J. Am. Chem. Soc.* **2003**, *125*, 3202–3203.
(24) Le Narvor, N.; Lapinte, C. *J. Chem. Soc., Chem. Commun.* **1993**, 357–359.
(25) Horn, C.; Martin-Alvarez, J. M.; Gladysz, J. A. *Organometallics* **2002**, *21*, 5386–5393.
(26) Coat, F.; Lapinte, C. *Organometallics* **1996**, *15*, 477–480.
(27) Ghazala, S. I.; Paul, F.; Toupet, L.; Roisnel, T.; Hapiot, P.; Lapinte, C. *J. Am. Chem. Soc.* **2006**, *128*, 2463–2476.
(28) Weyland, T.; Costuas, K.; Toupet, L.; Halet, J.-F.; Lapinte, C. *Organometallics* **2000**, *19*, 4228–4239.
(29) Le Stang, S.; Paul, F.; Lapinte, C. *Organometallics* **2000**, *19*, 1035–1043.
(30) Paul, F.; Lapinte, C. *Coord. Chem. Rev.* **1998**, *178−180*, 431–509.
(31) Paul, F.; Lapinte, C. In *Unusual Structures and Physical Properties in Organometallic Chemistry*; Gielen, M., Willem, R., Wrackmeyer, B., Eds.; Wiley: London, 2002; pp 220−291.
(32) Lapinte, C. *J. Organomet. Chem.* **2008**, *693*, 793–801.
(33) Roué, S.; Lapinte, C.; Bataille, T. *Organometallics* **2004**, *23*, 2558–2567.
(34) Sakurai, H. *J. Organomet. Chem.* **1980**, *200*, 261–286.
(35) West, R. *J. Organomet. Chem.* **1986**, *300*, 327–346.
(36) West, R. In *Comprehensive Organometallic Chemistry II*; Wilkinson, G., Stone, F. G. A., Abel, E. W., Eds.; Pergamon Press: London, 1995; Vol. 2, p 77.
(37) Patai, S.; Rappoport, Z. *The Chemistry of Organic Silicon Compounds*; Wiley: Chichester, U.K., 1989.
(38) Patai, S.; Rappoport, Z. *The Chemistry of Organic Silicon Compounds*; Wiley: Chichester, U.K., 1998; Vol. 2.
(39) Pitt, C. G. *Homoatomic Rings, Chains and Macromolecules of Main Group Elements*; Elsevier: New York, 1977; p 203.
(40) Dement'ev, V. V.; Cervantes-Lee, F.; Parkanyi, L.; Sharma, H. K.; Pannell, K. H. *Organometallics* **1993**, *12*, 1983–1987.
(41) Mignani, G.; Barzoukas, M.; Zyss, J.; Soula, G.; Balegroune, F.; Grandjean, D.; Josse, D. *Organometallics* **1991**, *10*, 3660–3668.
(42) Hissink, D.; Van Hutten, P. F.; Hadziioannou, G.; Van Bolhuis, F. *J. Organomet. Chem.* **1993**, *454*, 25–34.
(43) Sharma, H. K.; Pannell, K. H.; Ledoux, I.; Zyss, J.; Ceccanti, A.; Zanello, P. *Organometallics* **2000**, *19*, 770–774.
(44) Rautz, H.; Stüger, H.; Kickelbick, G.; Pietzsch, C. *J. Organomet. Chem.* **2001**, *627*, 167–178.
(45) Hamon, P.; Toupet, L.; Hamon, J.-R.; Lapinte, C. *Organometallics* **1996**, *15*, 10–12.

Chart 1

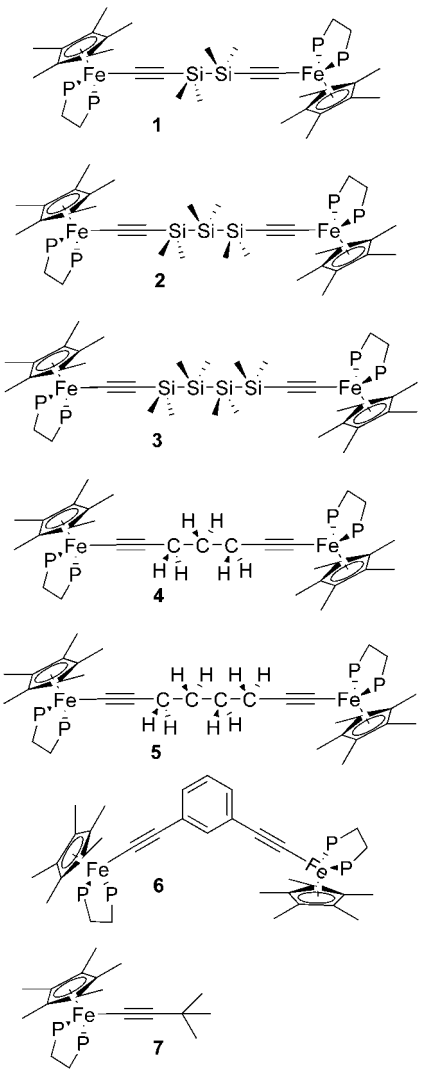

Scheme 1

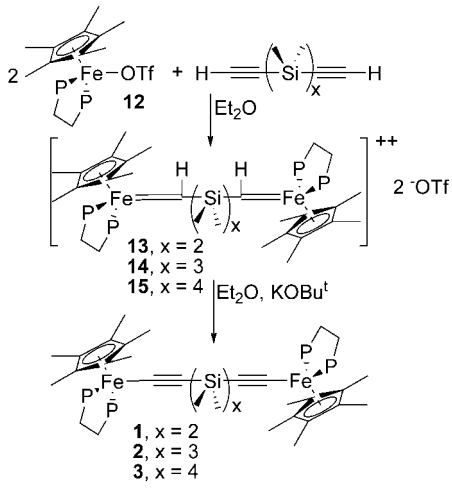

spectroscopies (see the Experimental Section). During the time needed to record the ^{13}C NMR spectra in acetone-d_6, 25−50% of each of the bimetallic complexes **13**−**15** was transformed into **9**. The target bis(alkynediyl) derivatives **1**−**3** were obtained by treatment of suspensions of **13**−**15**, respectively, in diethyl ether with potassium *tert*-butoxide. Extraction of the reaction mixtures with toluene allowed the isolation of compounds **1**−**3** as orange powders in yields ranging from 76 to 91%. The neutral complexes were characterized by the usual spectroscopies, while X-ray data obtained for **1** and **3** confirmed the proposed structures (Figure 1). Satisfactory elemental analyses were also obtained for these new compounds.

The complexes were also characterized by a typical infrared absorption at 1972, 1968, and 1968 cm^{-1} (KBr) for **1**, **2**, and **3** respectively, which corresponds to the stretching vibration mode of the C≡C bonds coordinated to the iron centers (Table S1 in the Supporting Information).[33] In previous work on Fe(II) acetylides, (Cp*)(dppe)Fe(C≡C−C_6H_4−X), it was observed that the stretching frequency for the triple bond ($\nu_{C\equiv C}$) depends on the electronic nature of the appended substituent X and ranges from 2037 cm^{-1} (X = NO_2) to 2060 cm^{-1} (X = OMe); it was also found that replacement of the phenyl ring by a 9,10-anthracene fragment increases the sensitivity to the substituent effect, allowing the observation of the C≡C stretch at a frequency as low as 1986 cm^{-1} (X = CN).[46,47] The variation of the C≡C bond stretching frequency was rationalized in terms of electronic structure using a valence-bond formalism by considering that electron-withdrawing substituents in Fe(II) acetylides favor the cumulenic character of the alkynyl bridge. In this context, the stretching frequencies found for the C≡C bonds of **1**−**3** are the lowest frequencies ever observed for Fe(II) acetylide complexes.[48] This result probably reveals the importance of the $\sigma-\pi$ conjugation (hyperconjugation) between the Si−Si σ bond and the adjacent C≡C π-symmetric orbitals in the description of the electronic structure of the ground state of these complexes.

2. Molecular Structures of 1 and 3. There is one precedent involving all-carbon-bridged metal centers containing methylene groups,[33] but no compounds containing −C(sp)− chains incorporating Si−Si bonds between alkynyl fragments and having two end-capping organometallic moieties have been structurally characterized to date. Nevertheless, one can mention that the M−C≡C−$(CH_2)_x$−C≡C−M (M = Si) moiety in some sterically hindered compounds was characterized by X-ray analysis.[49−52] Crystals of **1** and **3** suitable for X-ray analysis were grown by slow diffusion of pentane into a saturated toluene solution of the complexes. The unit cells of **1** and **3** contain 1 and 24 molecules, respectively. The molecular structures are shown in Figure 1, the X-ray data conditions summarized in the Experimental Section, and the crystal data, data collection, and structure refinement parameters given in Table S2 in the Supporting Information. Complex **1** crystallizes in the triclinic space group $P\bar{1}$, while its analogue **3** belongs to the tetragonal space group $I4_1/a$. Complex **3** crystallizes with two-thirds of a toluene molecule. As is invariably observed for all of the members of the Cp*(dppe)Fe−C≡C family of complexes, the

(46) Denis, R.; Toupet, L.; Paul, F.; Lapinte, C. *Organometallics* **2000**, *19*, 4240–4251.
(47) de Montigny, F.; Argouarch, G.; Roisnel, T.; Toupet, L.; Lapinte, C.; Lam, S. C.-F.; Tao, C.-H.; Yam, V. W.-W. *Organometallics* **2008**, *27*, 1912–1923.
(48) Paul, F.; Mevellec, J.-Y.; Lapinte, C. *Dalton Trans.* **2002**, 1783–1790.
(49) Haberhauer, G.; Rominger, F.; Gleiter, R. *J. Chem. Soc., Perkin Trans.2* **1999**, 947–950.
(50) Haberhauer, G.; Gleiter, R.; Irngartiner, H.; Oeser, T.; Rominger, F. *J. Chem. Soc., Perkin Trans.2* **1999**, 2093–2097.
(51) Stahr, H.; Gleiter, R.; Haberhauer, G.; Irngartiner, H.; Oeser, T. *Chem. Ber.* **1997**, *130*, 1807–1811.
(52) Gleiter, R.; Stahr, H.; Stadtmuller, F.; Irngartiner, H.; Pritzkow, H. *Tetrahedron Lett.* **1995**, *36*, 4603–4606.

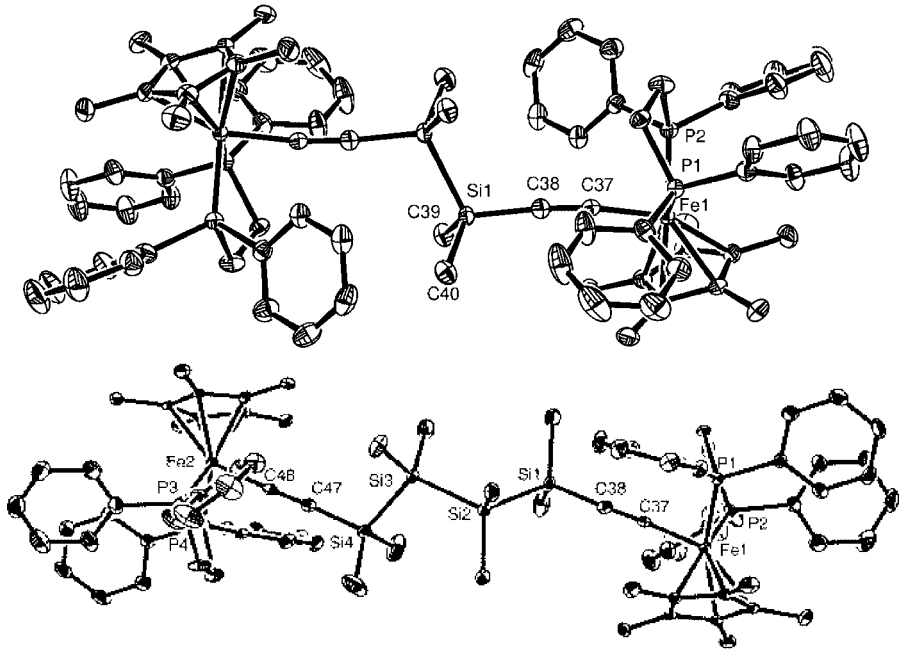

Figure 1. Molecular structures of (top) **1** and (bottom) **3**·$^2/_3C_7H_8$, showing thermal ellipsoids at the 50% probability level. Hydrogen atoms and (for **3**) toluene molecules have been removed for clarity.

Table 1. Selected Bond Distances and Angles for **1** and **3**·$^2/_3C_7H_8$

	1	**3**·$^2/_3C_7H_8$
Bond Distances (Å)		
Fe(1)−P(1)/Fe(2)−P(3)	2.1708(9)	2.1756(11)/2.1811(11)
Fe(1)−P(2)/Fe(2)−P(4)	2.1767(9)	2.1699(11)/2.1655(11)
Fe(1)−C(1−5)/Fe(2)−C(75−79)	2.120(3)	2.116(3)/2.140(3)
Fe(1)−C(37)/Fe(2)−C(48)	1.888(3)	1.898(4)/1.887(4)
C(37)−C(38)/C(47)−C(48)	1.233(5)	1.225(5)/1.220(5)
C(38)−Si(1)/Si(4)−C(47)	1.814(3)	1.811(4)/1.817(4)
Si(1)−Si(2)/Si(3)−Si(4)	2.3332(18)	2.3271(15)/2.3427(14)
Si(2)−Si(3)		2.3633(14)
Fe−Fe	11.07	14.51/14.69
Bond Angles (deg)		
P(1)−Fe(1)−P(2)/P(3)−Fe(2)−P(4)	85.86(3)	84.93(4)/83.75(4)
P(1)−Fe(1)−C(37)/P(3)−Fe(2)−C(48)	83.43(9)	85.26(11)/85.48(11)
P(2)−Fe(1)−C(37)/P(4)−Fe(2)−C(48)	88.12(10)	85. 70(11)/84.60(11)
Fe(1)−C(37)−C(38)/Fe(2)−C(48)−C(47)	172.7(3)	177.0(3)/177.0(3)
C(37)−C(38)−Si(1)/C(48)−C(47)−Si(4)	173.1(3)	177.4(3)/175.1(3)
C(38)−Si(1)−Si(2)/C(47)−Si(4)−Si(3)	110.41(12)	109.71(13)/110.80(12)
Si(1)−Si(2)−Si(3)		112.93(5)
Si(2)−Si(3)−Si(4)		110.97(5)

two metal moieties adopt pseudooctahedral geometries with bond lengths and angles in previously established ranges.[14,15,30,46,53,54]

Various data in Table 1 are relevant to the results discussed below. For example, the Fe−C_α≡ bond distances, which are the same in **1** and **3**, are slightly shorter than the analogous iron−C(sp) bond lengths in the closely related complex **4** and significantly shorter than the iron−C(sp^3) bond length [2.003(4) Å].[55,56] A similar Fe−C distance was observed in the case of a binuclear complex having the same endgroups connected by a bis(diethynyl)-4,4′-biphenyl spacer [1.888(4) Å],[27] and shorter distances were found for the bimetallic complexes bridged by all-carbon $-C_x-$ chains ($x = 4$, 1.884/1.889 Å;[57] $x = 8$, 1.862/1.864 Å).[15] While the Si−Si bond lengths have the expected value for single bonds, the Si−C(sp) bonds observed for **1** and **3** are rather short.[58] The geometry around the silicon atoms is approximately tetrahedral. The angle formed between the ethynyl triple bond and the C−Si bond, which ranges from 173 to 177°, deviates only slightly from linearity. Taken together, these data can be rationalized by hyperconjugation-type $\sigma-\pi$ interactions within the C≡C−Si moieties of **1** and **3**. The coplanar arrangement of the planes defined by the C−Si−Si chains in complex **1** [as indicated by the ≡C(38)−Si−Si−C(38)≡ dihedral angle of 180°] is favorable for metal−metal interactions along the Fe−C≡C−Si−Si−C≡C−Fe axis. In compound **3**, the arrangement is possibly less favorable for metal−metal interactions across the hybrid carbon−silicon bridge. Indeed, the planes defined by the C−Si−Si chains are still roughly coplanar (161°), as are the planes defined by the C−Si−Si−C dihedral angles (170 and 176°), but the arrangement around the central Si−Si bond, with a −Si−Si−Si−Si− dihedral angle of 113°, is less favorable. In the light of the IR data and molecular structure analysis, it appears that the Fe−C≡C−Si interactions are rather strong but that electronic interactions are probably weakly conveyed across the Si−Si bonds. The presence of tetrahedral silicon atoms in the bridge allows flexibility of the linker, and the metal−metal distances in **1** (11.07 Å) and **3**

(53) Weyland, T.; Lapinte, C.; Frapper, G.; Calhorda, M. J.; Halet, J.-F.; Toupet, L. *Organometallics* **1997**, *16*, 2024–2031.
(54) Coat, F.; Guillevic, M.-A.; Toupet, L.; Paul, F.; Lapinte, C. *Organometallics* **1997**, *16*, 5988–5998.
(55) Roger, C.; Toupet, L.; Lapinte, C. *J. Chem. Soc., Chem. Commun.* **1988**, 713–715.
(56) Roger, C.; Hamon, P.; Toupet, L.; Rabaâ, H.; Saillard, J.-Y.; Hamon, J.-R.; Lapinte, C. *Organometallics* **1991**, *10*, 1045–1054.
(57) Jiao, H.; Costuas, K.; Gladysz, J. A.; Halet, J.-F.; Guillemot, M.; Toupet, L.; Paul, F.; Lapinte, C. *J. Am. Chem. Soc.* **2003**, *125*, 9511–9522.
(58) Shaw-Taberlet, J. A.; Hamon, J.-R.; Roisnel, T.; Lapinte, C.; Flock, M.; Mitterfellner, T.; Stueger, H. *J. Organomet. Chem.* **2007**, *692*, 2046–2055.

Table 2. Electrochemical Data for **1**−**3** and Selected Compounds[a]

compd	$E_1°$	$(i_{pa}/i_{pc})_1$	$E_2°$	$(i_{pa}/i_{pc})_2$	$\Delta E°$	K_c	ref
1	−0.218	1	−0.081	1	0.137	227	this work
2	−0.203	1	−0.103	1	0.100	59	this work
3	−0.192	1	−0.104	1	0.088	33	this work
4	−0.336	1	−0.216	1	0.120	96	33
5	−0.320	1	−0.240	1	0.080	24	33
6	−0.225	1	−0.100	1	0.125	130	63
7	−0.28	1					64

[a] Potentials in CH_2Cl_2 (0.1 M [*n*-Bu_4N][PF_6]; 20 °C, glassy carbon electrode, sweep rate 0.100 V s^{-1}) are given in V vs SCE; the ferrocene−ferrocenium couple (0.460 V vs SCE) was used as an internal calibrant for the potential measurements.

(14.51/14.69 Å) are 10 and 15% shorter, respectively, than the sums of the bond distances in the Fe−Fe assemblies.

3. Cyclic Voltammetry of 1−3. The initial scan in the cyclic voltammogram of complex **1** from −0.6 to 0.4 V [vs the standard calomel electrode (SCE)] is characterized by two distinct, well-resolved reversible one-electron waves. This indicates that the neutral dimer undergoes two successive one-electron oxidations to yield the mono- and dications, respectively. As the number of silicon atoms in the hybrid bridge increases, the wave separation decreases in **2**, and the waves merge into a single two-electron reversible wave for **3** (see Figure S2 in the Supporting Information). As the anodic and cathodic currents are strictly identical, the electron-deficient species are apparently stable at the glassy carbon electrode. The determination of the two standard potentials $E_1°$ and $E_2°$ was straightforward for **1** (Table 2). When the separation between the two waves is too small, below the limit of the resolution of the cyclic voltammogram, the redox potentials cannot be determined as the midpoints between the anodic and cathodic peaks of the corresponding one-electron waves. However, their determination can be derived from the location of the midpoint between the anodic and cathodic peaks of the two-electron wave and the distance between them (ΔE_p), provided the kinetics of the electron-transfer processes do not affect the CV response.[59−62] This condition was checked by investigating the variation of ΔE_p as a function of the scan rate, and only negligible variations were observed for scan rates below 1 V s^{-1}. Thus, ΔE_p tends toward a limit (85 mV) that corresponds to the thermodynamics of the electron transfer; this limit leads to a value of 62 mV for the difference $\Delta E° = E_2° - E_1°$ (using a working curve after simulation of the voltammogram). Thus, the equilibrium constant K_c for the comproportionation reaction

$$\{[M^{red}]-B-[M^{red}]\}^{n+} + \{[M^{ox}]-B-[M^{ox}]\}^{(n+2)+} \overset{K_c}{\rightleftharpoons} 2\{[M^{red}]-B-[M^{ox}]\}^{(n+1)+} \quad (1)$$

where −B− represents the bridge between the metal atoms, ranges from 227 for **1** to 33 for **3**, according to eq 2:

$$\Delta E° = E_2° - E_1° = -\frac{RT}{F} \ln K_c \quad (2)$$

where R is the gas constant and F is the Faraday constant.

The electrochemical data found for the dinuclear compounds **1**−**3** are collected in Table 2 and compared to the results obtained for weakly coupled binuclear complexes that possess an alkynediyl bridge incorporating either methylene groups (**4** and **5**) or a 1,3-connected arene ring (**6**). From this comparison, it appears that complexes **1**−**3** are oxidized at slightly more positive potentials than complexes **4** and **5**, suggesting that the hybrid bridge $-C\equiv C-(Si(CH_3)_2)_x-C\equiv C-$ can be regarded as electron-withdrawing with respect to the organic analogue $-C\equiv C-(CH_2)_x-C\equiv C-$. The potential difference $\Delta E°$ between the two redox events and the comproportionation constant K_c are both representative of the thermodynamic stability of the corresponding MV state relative to other redox states. Their magnitudes are determined by the sum of several energetic factors relating to the stabilities of the reactant and product complexes, and it is important to keep in mind that a single redox event is not diagnostic of the absence of electronic communication between the redox centers.[32] The knowledge of K_c allowed the determination of the molar fractions of the species present in solution. In particular, when 1 equiv of the neutral complex is reacted with 1 equiv of one-electron oxidizing reagent, the molar fractions of the MV species are approximately 0.9, 0.8, and 0.7 for **1**, **2**, and **3**, respectively.

4. Isolation of the Radical Cations 1[X]$_2$, 2[X]$_2$, and 3[X]$_2$. On the basis of the full reversibility of the CV waves, the doubly oxidized complexes **1**[X]$_2$ −**3**[X]$_2$ were considered as accessible synthetic targets. According to a well-established procedure, complexes **1** and **3** were first reacted with 1.95 equiv of [$(C_5H_5)_2$Fe][PF_6] in tetrahydrofuran (THF).[33] However, the corresponding bis[iron(III)] complexes could not be obtained by this procedure. The decomposition of the starting material was attributed to a possible reaction between the silicon groups and the hexafluorophosphate counteranion. Alternatively, compounds **1**−**3** were treated at $T < -20$ °C with 2 equiv of [$(C_5H_5)_2$Fe][BPh_4] in CH_2Cl_2 or 2 equiv of Ag[B(3,5-$(CF_3)_2C_6H_3)_4$)] in diethyl ether. The initial orange solution progressively turned dark-red. After completion of the reactions, the solutions were filtered into a Schlenk tube containing pentane to precipitate the salts. The solid residues were isolated by removal of the solvent by filtration and drying under vacuum followed by rapid washings with cold pentane. On the basis of the IR spectra, each of which displayed a single C≡C bond stretch that was slightly shifted toward lower frequencies (5−10 cm^{-1}) with respect to that of the neutral compound, and the cyclic voltammograms, which were absolutely identical to those of the iron(II) parent complexes, these compounds can be regarded as the targeted dioxidized complexes **1**[X]$_2$−**3**[X]$_2$ [X = BPh_4, B(3,5-$(CF_3)_2C_6H_3)_4$]. In the solid state, the samples were apparently stable under argon atmosphere when stored below −20 °C. The thermal stability of these salts increases with the number of silicon atoms. Indeed, compound **3**[X]$_2$ is stable for a few hours at 20 °C, while **2**[X]$_2$ is stable for 5 min at 20 °C (a time long enough for weighing of the sample) and **1**[X]$_2$ decomposes in less than 2 min at 20 °C. As a control experiment, a THF solution of the most stable derivative, **3**[BPh_4]$_2$, was treated with 2 equiv of cobaltocene at −80 °C, causing a slow color change from purple to orange. After workup, the corresponding complex **3** was isolated in 86% yield and identified by comparison of its CV, IR, and ^{1}H and ^{31}P NMR data to those of an authentic sample.

It appeared that preparations of **1**[X]$_2$−**3**[X]$_2$ were probably successfully and almost quantitatively achieved. However, elemental analyses of the samples revealed the presence of traces of impurities, and further purifications were precluded by the chemical instability of these complexes in solution. The solution always progressively turned dark-green, indicating that decom-

(59) Myers, R. L.; Shain, I. *Anal. Chem.* **1969**, *41*, 980.
(60) Hapiot, P.; Kispert, L. D.; Konovalov, V. V.; Savéant, J.-M. *J. Am. Chem. Soc.* **2001**, *123*, 6669–6667.
(61) Andrieux, C. P.; Savéant, J.-M. *Electroanal. Chem.* **1974**, *57*, 27–33.
(62) Guerro, M.; Carlier, R.; Boubekeur, K.; Lorcy, D.; Hapiot, P. *J. Am. Chem. Soc.* **2003**, *125*, 3159–3167.

Table 3. EPR Parameter Values for Compounds $\mathbf{1}^{n+}-\mathbf{3}^{n+}$ Measured at 66 K and for Closely Related Compounds Measured at 77 K

compd	g_1 (a_1)[a]	g_2 (a_2)[a]	g_3	g_{iso}[b]	Δg[c]	ref
$\mathbf{1}^+$	1.978 (13)	2.032	2.444	2.151	0.466	this work
$\mathbf{1}^{2+}$	1.978	2.028	2.443	2.150	0.468	this work
		$\Delta m_s = \pm 2$, $g = 4.254$, $\Delta H_{pp} = 47$ G				
$\mathbf{2}^{2+}$	1.985	1.985	2.440	2.14	0.49	this work
		D[d] $= 250$ G, E[e] $= 50$ G, $\Delta m_s = \pm 2$, $g = 4.37$, $\Delta H_{pp} = 300$ G				
$\mathbf{3}^+$	1.977 (13)	2.013 (28)	2.463	2.151	0.486	this work
$\mathbf{3}^{2+}$	1.977 (18)	2.030 (28)	2.445	2.155	0.489	this work
		$\Delta m_s = \pm 2$, $g = 4.261$, $\Delta H_{pp} = 40$ G				
$\mathbf{4}^+$	1.981 (15)	2.037 (12)	2.433	2.150	0.452	33
$\mathbf{4}^{2+}$		$\Delta m_s = \pm 1$, $g = 2.2$, $\Delta H_{pp} = 600$ G				33
		$\Delta m_s = \pm 2$, $g = 4.267$				
$\mathbf{5}^+$	1.979	2.037	2.438	2.151	0.459	33
$\mathbf{5}^{2+}$		$\Delta m_s = \pm 1$, $g = 2.2$, $\Delta H_{pp} = 700$ G				33
		$\Delta m_s = \pm 2$, signal not found				
$\mathbf{7}^{+}$[f]	1.980	2.032	2.505	2.170	0.530	64

[a] In gauss. [b] $g_{iso} = (g_1 + g_2 + g_3)/3$. [c] $\Delta g = g_3 - g_1$. [d] Axial anisotropy (see ref 69). [e] Rhombic anisotropy (see ref 69). [f] [Cp*(dppe)FeC≡C−*t*-Bu][PF_6].

position processes took place. Spectroscopic analyses indicated that many impurities were formed, and the mononuclear vinylidene **9** was the only identified organometallic species. The three dications were characterized by IR and ESR. In addition, variable-temperature magnetic susceptibility measurements were carried out with compounds **2**[BPh_4]$_2$ and **3**[BPh_4]$_2$, while the derivative **3**[B(3,5-$(CF_3)_2C_6H_3)_4$]$_2$ was identified by electrospray ionization mass spectrometry (ESI MS).

5. Glass EPR Spectroscopy and Solid-State Magnetic Susceptibility. Compounds **1** and **3** were reacted with less than 1 equiv of [$(C_5H_5)_2$Fe][BPh_4] in a 1:1 THF/MeTHF mixture at −80 °C, providing a red solution that was transferred into an EPR tube before being cooled to 77 K. The X-band EPR spectra of the monocations **1**[BPh_4] and **3**[BPh_4] run at 66 K displayed three well-resolved features corresponding to the components of the **g** tensors (see Figure S3 in the Supporting Information), characteristic of d^5 low-spin Fe(III) in a pseudooctahedral environment. The *g* values extracted from the spectra are collected in Table 3. For both complexes, the good resolution of the spectra allowed the observation of the superhyperfine coupling with two phosphorus nuclei, clearly establishing the localization of the unpaired electron on a single metal center on the EPR time scale. For the MV compounds of the Cp*(dppe)Fe series, it has been suggested that the anisotropy tensor $\Delta\mathbf{g}$ decreases as the rate of the intramolecular electron transfer (ET) increases. The values found for **1**[BPh_4] and **3**[BPh_4] are very close, suggesting that the ET rate slowly decreases with the number of Si−Si bonds. One can also note that these values are very close to those previously found for complexes **4**[PF_6] and **5**[PF_6], indicating that the ET rate is probably on the same order of magnitude in the carbon and hybrid series. However, this comparison must be made with caution. Indeed, for these Fe(III) radicals, EPR anisotropy arises essentially from spin−orbit coupling. Roughly, the more ligand-centered the unpaired electron is, the less anisotropic the EPR signal, and the associated g_{iso} values become concomitantly closer to the g_e value ($g_e = 2.0023$).[65] Further analysis of the EPR data requires a comparison between mononuclear models containing all-carbon and hybrid ligands to evaluate the role of the $Si(CH_3)_2$ groups on the "metal-versus-bridge"character of the unpaired electron. A synthetic route toward these compounds is the subject of active research.[66]

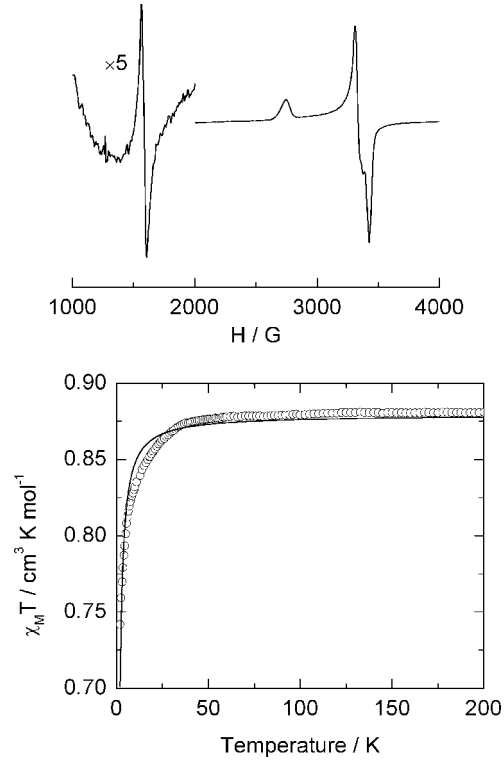

Figure 2. (top) X-band EPR spectrum of **3**[BPh_4]$_2$ recorded at 66 K and (bottom) thermal dependence of $\chi_M T$ (circles) with the best-fit curve from eq 4 (solid line).

THF solutions of the dicationic complexes **1**[BPh_4]$_2$−**3**[BPh_4]$_2$, prepared either from isolated compounds (see above) or by in situ treatment of complexes **1**−**3** with 2 equiv of [$(C_5H_5)_2$Fe][BPh_4] in THF at −80 °C, provided similar EPR spectra. The low-temperature EPR spectrum of the dicationic compound **3**[BPh_4]$_2$ displays well-resolved structure, with three components for the $\Delta m_s = \pm 2$ transitions (Figure 2, top). This finding is surprising and unprecedented in the Cp*(dppe)Fe series. Indeed, diradicals usually show unresolved

(63) Weyland, T.; Costuas, K.; Mari, A.; Halet, J.-F.; Lapinte, C. *Organometallics* **1998**, *17*, 5569–5579.
(64) Connelly, N. G.; Gamasa, M. P.; Gimeno, J.; Lapinte, C.; Lastra, E.; Maher, J. P.; Le Narvor, N.; Rieger, A. L.; Rieger, P. H. *J. Chem. Soc., Dalton Trans.* **1993**, 2575–2578.
(65) Paul, F.; Toupet, L.; Thépot, J.-Y.; Costuas, K.; Halet, J.-F.; Lapinte, C. *Organometallics* **2005**, *24*, 5464–5478.
(66) Lapinte, C.; Hamon, J.-R.; Stüger, H. Work in progress.

broad signals with peak-to-peak separations (ΔH_{pp}) as large as 600 G.[33,63] The broadening of the signal was attributed to a dominant electron−electron relaxation process.[33,63,67] In the present case, conformational gating of exchange and hyperfine coupling parameters would explain the line width of the EPR spectra, as has been proposed for spirobiradicals.[68] Equally remarkable, the superhyperfine coupling with phosphorus nuclei manifests itself in the spectrum of **3**$[BPh_4]_2$. Moreover, the $\Delta m_s = \pm 2$ transition characteristic of a spin multiplicity greater than 2 (a triplet in our case) is clearly observed at $g = 4.261$ (Figure 2, top). The spectrum of **2**$[BPh_4]_2$ also displays the half-field feature, but in this case the signal is broader and can only be observed with a larger amplification of the signal (Figure S5 in the Supporting Information). Additionally, fine structure is clearly visible in the $g = 2.00$ region in the low-temperature spectrum of **2**$[BPh_4]_2$, reflecting the zero-field splitting of the m_s components of the triplet state (Table 3). These interesting results clearly demonstrate that magnetic exchange interactions between the two iron(III) spin carriers can be mediated through two and even three silicon−silicon bonds.

Solid-state magnetization measurements confirm the existence of superexchange interactions between the iron(III) spins through the Si−Si bonds. The temperature dependence of the $\chi_M T$ product (where χ_M is the molar magnetic susceptibility and T the temperature in Kelvin) of a powdered sample of **3**$[BPh_4]_2$, is plotted against T in the bottom panel of Figure 2. At room temperature, $\chi_M T$ is equal to 0.86 cm^3 K mol^{-1}, which is close to the spin-only value (0.87 cm^3 K mol^{-1}) expected for two uncoupled $S = {}^1/_2$ spins with $g_{iso} = 2.155$. As the temperature decreases, $\chi_M T$ remains quasi-constant down to 50 K and then decreases more and more rapidly, indicative of antiferromagnetic interactions between the spin carriers. The experimental data can be reproduced by considering a Heisenberg-type superexchange interaction between two $S = {}^1/_2$ spins localized on iron(III) centers. In the presence of an external magnetic field, the Hamiltonian is then expressed by eq 3 if the Zeeman anisotropy is neglected:

$$\hat{H} = -J\hat{\mathbf{S}}_1 \cdot \hat{\mathbf{S}}_2 + g_{iso}\beta \mathbf{H} \cdot (\hat{\mathbf{S}}_1 + \hat{\mathbf{S}}_2) \quad (3)$$

where J is the superexchange interaction parameter, $\hat{\mathbf{S}}_1$ and $\hat{\mathbf{S}}_2$ are the spin operators on the iron(III) sites, β is the Bohr magneton, and **H** is the magnetic field. The Bleaney−Bowers equation (eq 4)[70] reproduces the thermal variation of the magnetic susceptibility:

$$\chi_M T = \frac{2N g_{iso}^2 \beta^2}{k[3 + \exp(-J/kT)]} \quad (4)$$

The best agreement with the experimental data was obtained with $J = -0.97(2)$ cm^{-1} and $g_{iso} = 2.165(1)$, clearly establishing that superexchange interaction propagates through the three Si−Si bonds. It must be argued that the agreement is not optimum. However, because of the thermal instability of the compound, a partial decomposition of the sample during the preparation cannot be excluded. Identical measurements and theoretical treatment were also performed on **2**$[BPh_4]_2$ (Figure S6 in the Supporting Information). Despite the fact that the shorter the Si−Si chain, the more thermally unstable the sample, stronger interactions between the iron(III) centers were measured even at room temperature ($J = -1.70$ cm^{-1}). It should be noted that the thermal instability of the samples was clearly probed by SQUID measurements. Indeed, the magnetization evolves with time above 200 K, and the shorter the Si−Si chain, the faster the evolution.

Table 4. UV−Vis Absorption Data for Complexes $\mathbf{1}^{n+}$−$\mathbf{3}^{n+}$ (n = 0−2) in CH_2Cl_2 at 298 K

compd	λ_{max} [nm] (ε [M^{-1} cm^{-1}])
1	260 (sh, 50 000), 360 (6000),[a] 420 (4000), 510 (sh, 1200)
$\mathbf{1}^+$	360 (6000),[a] 404 (3800), 540 (2400)
$\mathbf{1}^{2+}$	360 (6000),[a] 410 (3600), 516 (1600)
2	260 (sh, 50 000), 396 (1800),[a] 410 (sh, 3600), 510 (sh, 1000)
$\mathbf{2}^+$	396 (1800),[a] 414 (2000), 542 (1400)
$\mathbf{2}^{2+}$	396 (1800),[a] 432 (2200), 542 (2400)
3	260 (sh, 50 000), 402 (3500),[a] 410 (sh, 3300), 510 (sh, 800)
$\mathbf{3}^+$	402 (3500),[a] 412 (3300), 530 (1800), 640 (sh)
$\mathbf{3}^{2+}$	402 (3500),[a] 432 (4000), 546 (4800)

[a] Isosbestic point.

6. Electronic Absorption Spectroscopy. The UV−vis spectra of complexes **1**−**3** were recorded at 20 °C in CH_2Cl_2, and the characteristic data are collected in Table 4. The three spectra are very similar. Besides the intense absorptions below 300 nm that present shoulders at 260 nm, which are assignable to intraligand transitions involving the C_5Me_5 and phosphine ligands, the electronic absorptions of the neutral species exhibit two weakly intense shoulders in the visible range at 410 and 510 nm. With reference to the related compounds **4** and **5**, which also show low-energy absorptions at 374 and 430 nm, the low-energy bands of **1**−**3** observed in the visible range are tentatively assigned to $d\pi(Fe) \rightarrow \pi^*(C{\equiv}C)$ metal-to-ligand charge transfer (MLCT) transitions.[33,71] However, the important red shift observed for the band in the carbon−silicon hybrid series with respect to the compounds that incorporate methylene groups in their bridges suggests $\sigma-\pi$ hyperconjugation between the σ bond and the adjacent π-symmetric C≡C orbitals. It is also noteworthy that the transparency in the UV−vis range of the hybrid complexes **1**−**3** is very similar to that of their silicon-free counterparts **4** and **5**.

The UV−vis−NIR spectra of **1**$[OTf]_n$, **2**$[OTf]_n$, and **3**$[OTf]_n$ (n = 0−2) were collected using spectroelectrochemical methods. The UV−vis−NIR spectra were obtained with an optically transparent thin-layer electrosynthetic (OTTLE) cell with a standard design,[72] and the results are summarized in Tables 4 and 5. All of the measurements were carried out in CH_2Cl_2 (unless otherwise specified) containing 0.1 M [n-Bu_4N][OTf] as the supporting electrolyte. Not unexpectedly, the spectral profiles generated from the three compounds and their one- and two-electron oxidized forms are similar, with red-shift tendencies as the number of dimethylsilane groups increases. The 410 and 510 nm absorptions of the neutral species were used as references for determining the extinction coefficients of the oxidized forms.

Upon oxidation, two maxima arose in the visible range, while absorption bands with a complex shape were observed in the NIR region. The intensity maxima of the NIR bands correspond to monoelectronic oxidation of the starting material and were

(67) Paul, F.; Meyer, W. E.; Toupet, L.; Jiao, H.; Gladysz, J. A.; Lapinte, C. *J. Am. Chem. Soc.* **2000**, *122*, 9405–9414.
(68) Frank, N. L.; Clérac, R.; Sutter, J.-P.; Daro, N.; Kahn, O.; Coulon, C.; Green, M. T.; Golhen, S.; Ouahab, L. *J. Am. Chem. Soc.* **2000**, *122*, 2053–2061.
(69) Abragam, A.; Bleaney, B. *Electron Paramagnetic Resonance of Transition Ions*; Dover Publications: New York, 1970.
(70) Kahn, O. *Molecular Magnetism*; VCH: New York, 1993; p 380.
(71) Costuas, K.; Paul, F.; Toupet, L.; Halet, J.-F.; Lapinte, C. *Organometallics* **2004**, *23*, 2053–2068.
(72) Duff, C. M.; Heath, G. A. *Inorg. Chem.* **1991**, *30*, 2528–2535.

Table 5. NIR Data for **1**[OTf]−**3**[OTf] in CH_2Cl_2

compd	transition[a]	ν_{max} (cm^{-1})	ε (M^{-1} cm^{-1})	$\Delta\nu_{1/2,exptl}$ (cm^{-1})	$\Delta\nu_{1/2,theor}$ (cm^{-1})	H_{ab} (cm^{-1})	d_{ab} (Å)	α^2
1[OTf]	LF	5300	120	1100			11.07	
	IVCT	6400	1000	3700	3800	285		19.2×10^{-4}
2[OTf]	LF	5300	60				12.79	
	IVCT	6700	260	3800	3900	130		3.7×10^{-4}
2[OTf][b]	LF	5300	50					
	IVCT	7800	*c*	4200	4200	*c*		
3[OTf]	LF	5300	90	1200			14.51	
	IVCT	8500	60	4500	4400	64		0.6×10^{-4}

[a] $n > 1$. [b] A 40:60 dichloromethane/acetone mixture was used as the solvent. [c] Not determined.

used as an indicator of the completion of this process. The second one-electron oxidation reaction induced a decrease in the intensity of the bands in the NIR range accompanied by a blue shift. As the second oxidation took place, the intensity maxima in the visible range decreased for compound $\mathbf{1}^{n+}$ but continuously increased in the case of compounds $\mathbf{2}^{n+}$ and $\mathbf{3}^{n+}$. The two redox events observed for each of the three complexes in this series were almost chemically reversible at room temperature on the time scale of the experiment. Nevertheless, the reversibility was much better when the reduction was carried out after the first oxidation rather than after the second one, suggesting better chemical stability in solution for the MV species than for the dicationic compounds. In the three series of spectra, isosbestic points were observed at 360, 396, and 402 nm for $\mathbf{1}[OTf]_n$, $\mathbf{2}[OTf]_n$, and $\mathbf{3}[OTf]_n$, respectively. These isobestic points indicate that neutral, mono-oxidized, and dioxidized species possess the same extinction coefficient for these particular wavelengths and confirm that the decomposition of the species generated in situ is not significant on the time scale of the experiment.

The two bands near 420 and 540 nm with intensities that increased upon oxidation can be ascribed to ligand-to-metal charge transfer (LMCT) transitions. In the related complexes $[Cp^*(dppe)Fe{-}C{\equiv}C{-}C_6H_4X][PF_6]$, the $\pi(C{\equiv}C) \rightarrow d\pi(Fe)$ LMCT transitions are observed at lower energies (X = H, 575 and 663 nm).[63,65] In contrast, in the case of complexes $\mathbf{4}[PF_6]_n$ and $\mathbf{5}[PF_6]_n$ ($n = 1, 2$), the observed blue shift ($\mathbf{4}[PF_6]$, 426 nm) was attributed to the restriction of the π system to alkynyl fragments.[33] The intermediate energies found for the iron(III) complexes in the hybrid series also support $\sigma-\pi$ hyperconjugation between the σ bond and the adjacent π-symmetric C≡C orbitals.

The spectra of the neutral complexes **1**−**3** do not contain any absorption bands in the NIR range. In contrast, the associated MV and dioxidized species both present characteristic absorptions. The spectra of the homovalent iron(III) diradical dications $\mathbf{1}-\mathbf{3}[OTf]_2$ display an absorption band centered around 5400 ± 100 cm^{-1} with weak intensity ($\varepsilon = 50 \pm 5$ M^{-1} cm^{-1}), corresponding to a forbidden ligand field (LF) transition specific to the Cp*(dppe)Fe(III) fragment.[65] In many cases, this iron(III) spectroscopic signature is too weak to significantly affect the intense intervalence charge transfer (IVCT) band of the Fe(II)−Fe(III) MV compounds already studied. However, when the intensity of the IVCT band is also weak, the contribution of the LF transition cannot be neglected.[27,28]

The bands exhibited by the MV compounds in the NIR range were analyzed by deconvolution using Gaussian functions, which revealed the presence of two overlapping transitions attributable to the MV species (Table 5). The band expected for the dications in equilibrium with the MV complexes at 5400 cm^{-1} was neglected. Indeed, because of the small molar fraction of the dication (maximum of 0.15) combined with the small extinction coefficient of the LF band, the introduction of this component into the calculations did not significantly change the result of the fits.

The lower-energy band found at 5300 cm^{-1} for each of the three MV complexes is attributed to an LF transition in the MV species, also called an interconfigurational (IC) transition by Meyer et al.,[73] by analogy to the absorptions invariably found in related Fe(III) aryl acetylides.[65] The second band located at higher energy is believed to correspond to an IVCT transition. As the values in Table 5 show, its width at half-height ($\Delta\nu_{1/2,exptl}$) is well in line with predicted values ($\Delta\nu_{1/2,theor}$) based on the Hush model (eq 5):[74−76]

$$\Delta\nu_{1/2,theor} = (2310\nu_{max})^{1/2} \quad (5)$$

It should be noted that the low-energy band is much narrower than predicted on the basis of eq 5 and presents values for $\Delta\nu_{1/2}$ in the range usually observed for LF transitions.[65]

The influence of the polarity of the solvent was also briefly investigated. However, the low solubilities of these complexes in common polar solvents, which favors the precipitation of the neutral species, drives the comproportionation equilibrium (eq 1) toward the left. Among the different attempts, an experiment in the OTTLE cell with **2** in a 2:3 CH_2Cl_2/acetone mixture was run. As shown in Figure 3, comparison of the spectra obtained in dichloromethane and the dichloromethane/acetone mixture establishes a solvatochromic behavior for the broad NIR absorption. Spectral data extracted from the experimental spectrum reveal that only the IVCT band is shifted (by ∼1100 cm^{-1} toward higher energy) when the polarity of the medium increases. There is also an increase of the bandwidth associated with the energy shift, as expected for an IVCT process obeying the Hush model. The low-energy band is apparently not sensitive to the polarity of the solvent, confirming that this transition has nothing to do with an IVCT process. This result is in agreement with the assignment of an IC transition for this band.

As the number of Si−Si σ bonds increases, the peak of the IVCT band is blue-shifted, evidencing that the photodriven metal−metal electron-transfer processes take place through the hybrid carbon−silicon connectors. The reorganization energy ($\lambda = \nu_{max}$) for this intramolecular process ranges from ∼6400 cm^{-1} for one Si−Si bond to ∼8500 cm^{-1} for three Si−Si bonds. One can also note that the reorganization energies associated with the electron transfer are larger for the MV complexes of the hybrid series than for the complexes $\mathbf{4}[PF_6]$ and $\mathbf{5}[PF_6]$. In

(73) Demandis, K. D.; Hartshorn, C. M.; Meyer, T. J. *Chem. Rev.* **2001**, *101*, 2655–2685.
(74) Hush, N. S. *Prog. Inorg. Chem.* **1967**, *8*, 391–444.
(75) Brunschwig, B. S.; Creutz, C.; Sutin, N. *Chem. Soc. Rev.* **2002**, *31*, 168–184.
(76) Nelsen, S. F. *Chem.−Eur. J.* **2000**, *6*, 581–588.

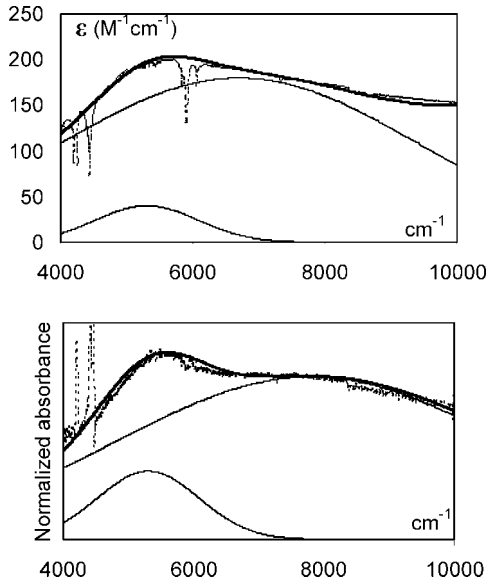

Figure 3. NIR spectra for **2**[PF_6] in (top) pure dichloromethane and (bottom) a 2:3 dichloromethane/acetone mixture.

addition, λ increases rather quickly with the number of Si−Si bonds. As a consequence, the Franck−Condon barrier should be higher for the silicon-containing compounds than for the silicon-free compounds **4**[PF_6] and **5**[PF_6].[5] Symmetrically, the electronic couplings H_{ab} derived from the IVCT band (eq 6),

$$H_{ab} = \frac{2.06\times10^{-2}}{d_{ab}}(\varepsilon_{max}\nu_{max}\Delta\nu_{1/2})^{1/2} \quad (6)$$

where d_{ab} is the through-space distance (in Å) between the redox-active iron centers, decrease in going from **1**[OTf] (285 cm^{-1}) to **3**[OTf] (64 cm^{-1}), as the number of Si−Si σ bonds increases from 1 to 3 (Table 5). Comparison of the H_{ab} values obtained for compounds **4**[PF_6] and **5**[PF_6] with those obtained here for the hybrid series roughly indicates that the electronic coupling is a factor of 2 smaller for each additional Si−Si bond and a factor of 3 smaller for the addition of an extra C−C single bond. In other words, our results suggest that $-Si(CH_3)_2-Si(CH_3)_2-$ units are slightly better than $-CH_2-CH_2-$ units as molecular conductors. The values of the α parameter (eq 7),

$$\alpha^2 = \left(\frac{H_{ab}}{\nu_{max}}\right)^2 \quad (7)$$

which represents the electronic delocalization (Table 5), are smaller than those obtained for **4**[PF_6] and **5**[PF_6], indicating that the electron density is focused on the iron centers. Moreover, as the number of Si−Si bonds increases, the spin density on the metal centers also increases.

Conclusion

In this contribution, the synthesis and characterization of a new family of binuclear acetylide complexes featuring electron-rich Cp*(dppe)Fe(C≡C) end groups connected by carbon−silicon hybrid connectors have been reported. To overcome the cleavage of the C−Si bonds during the complexation reaction with Cp*(dppe)FeCl, an original route using the triflate adduct Cp*(dppe)FeOTf in a nonpolar medium was found. The new hybrid derivatives [Cp*(dppe)Fe−C≡C$(Si(CH_3)_2)_x$C≡C−Fe(dppe)Cp*][BPh_4]$_n$ (x = 2−4, n = 0−2) were fully characterized in their neutral forms, including X-ray analysis for **1** and **3**. The data revealed the importance of the $\sigma-\pi$ conjugation (hyperconjugation) between the Si−Si σ bond and the adjacent C≡C π-symmetric orbitals in the description of the electronic structure of the ground states of these new compounds. Although well-resolved CV waves were only observed for **1**, the comproportionation constants of **2** and **3** could also be measured by CV. Despite the weak thermal stability of the mono- and dioxidized complexes, it was established by EPR spectroscopy and magnetization measurements that the superexchange interaction propagates through the Si−Si bonds ($J \approx 1$ cm^{-1}). Moreover, spectroelectrochemistry in an OTTLE cell allowed the observation of IVCT bands in the NIR domain, evidencing the existence of photodriven metal−metal electron-transfer processes between the iron centers (which are ∼11.0−14.5 Å apart) through the hybrid carbon−silicon bridges. These new complexes constitute original examples of well-behaved weakly coupled class-IIA organometallic MV compounds according to the Robin and Day classification.[77] The experimental data collected for these compounds present a high consistency with the two-level Hush model, which a posteriori justifies its use.[74,78−80]

Experimental Section

General Data. Manipulations of air-sensitive compounds were performed under an argon atmosphere using standard Schlenk techniques or in an argon-filled Jacomex 532 drybox. All of the glassware was oven-dried and degassed by vacuum or argon flow before use. FT-IR spectra were recorded using a Bruker IFS28 spectrophotometer (range 4000−400 cm^{-1}) on solids dispersed in KBr pellets. UV−vis spectra were recorded on a UVIKON XL spectrometer. ^1H, ^{13}C, and ^{31}P NMR spectra were recorded on a Bruker DPX200 multinuclear NMR spectrometer at ambient temperature, unless otherwise noted. ^{29}Si NMR spectra were run on a Bruker 300-MSL spectrometer. Chemical shifts (δ) are reported in parts per million relative to tetramethylsilane for ^1H, ^{13}C, and ^{29}Si NMR spectra and external 85% H_3PO_4 for ^{31}P NMR spectra. Coupling constants (J) are reported in hertz, and integrations are reported as numbers of protons. The following abbreviations are used to describe peak patterns: br = broad, s = singlet, d = doublet, t = triplet, q = quartet, m = multiplet. Mass spectra were run on an HP 5971/A/5890-II GC/MS coupling (HP 1 capillary column, length 25 m, diameter 0.2 mm, 0.33 m polydimethylsiloxane). EPR spectra were recorded on a Bruker EMX-8/2.7 (X-band) spectrometer equipped with liquid nitrogen cryostat. The magnetization was recorded with a Quantum Design MPMS SQUID magnetometer operating in the temperature range 2−300 K with a DC magnetic field of up to 5 T. The experimental data were corrected for the diamagnetism of the sample holder and the intrinsic diamagnetism of the materials as evaluated with Pascal's tables. Elemental analyses were conducted on a Thermo-FINNIGAN Flash EA 1112 CHNS/O analyzer by the Microanalytical Service of the Centre Régional de Mesures Physiques de l'Ouest (CRMPO) at the University of Rennes 1, France.

Materials. Reagent-grade toluene, THF, diethyl ether, and pentane were dried and deoxygenated by distillation from sodium/benzophenone ketyl. Dichloromethane was distilled under argon from P_2O_5 and then from Na_2CO_3. Cp*(dppe)FeCl,[56] Cp*(dppe)FeOTf,[45] $Cl(Si(CH_3)_2)_2Cl$ (1,2-dichlorotetramethyldisilane),[81] $Cl(Si(CH_3)_2)_3Cl$ (1,3-dichlorohexamethyltrisilane),[82]

(77) Robin, M. B.; Day, P. *Adv. Inorg. Chem. Radiochem.* **1967**, *10*, 247–422.
(78) Coropceanu, V.; Malagoli, M.; Andrés, J. M.; Brédas, J. L. *J. Am. Chem. Soc.* **2002**, *124*, 10519–10530.
(79) Creutz, C.; Newton, M. D.; Sutin, N. *J. Photochem. Photobiol., A* **1994**, *82*, 47–59.
(80) Evans, C. E. B.; Yap, G. P. A.; Crutchley, R. J. *Inorg. Chem.* **1998**, *37*, 6161–6167.

$Cl(Si(CH_3)_2)_4Cl$ (1,4-dichlorooctamethyltetrasilane),[82] $[(C_5H_5)_2Fe][PF_6]$ (ferrocenium hexafluorophosphate),[83] and $[(C_5H_5)_2Fe][BPh_4]$ (ferrocenium tetraphenylborate)[83] were prepared following published procedures. Ethynylmagnesium bromide (0.5 M solution in THF, Aldrich), methyl triflate, tetrabutylammonium triflate and potassium *tert*-butoxide (ACROS) were used as received without further purification. **Caution!** *Methyl trifluoromethanesulfonate is toxic and a suspected carcinogen; it should be handled in a well-ventilated fume hood.*

α,ω-Bis(ethynyl)permethyloligosilanes $[HC\equiv C-(Si(CH_3)_2)_x-C\equiv CH]$. General Procedure. A 0.5 M THF solution of HC≡CMgBr (2.1 equiv) was slowly added to a stirred solution of the corresponding α,ω-dichlorosilane in 150 mL of THF at −50 °C. Subsequently, the resulting mixture was stirred overnight at room temperature. After removal of the solvent under vacuum and addition of 200 mL of pentane, the salts were filtered and washed twice with pentane, and the solvent was stripped off again. The pure products were obtained from the resulting liquid residue by vacuum distillation.

$HC\equiv C-(Si(CH_3)_2)_2-C\equiv CH$.[84] $Cl(Si(CH_3)_2)_2Cl$ (18.5 g, 98.7 mmol) and 414 mL of 0.5 M HCCMgBr (207 mmol) gave 9.5 g (58%) of pure $HC\equiv C-(Si(CH_3)_2)_2-C\equiv CH$. Bp (80 mbar): 82 °C. ^1H NMR (200 MHz, C_6D_6): δ 2.53 (s, 2H, HC≡), 0.34 (s, 12H, $Si(CH_3)_2$). ^{29}Si NMR (59.62 MHz, pentane/D_2O): δ −36.7 ($Si(CH_3)_2$). MS (70 eV) *m/z* (rel. int.): 166 (M^+, 0.8).

$HC\equiv C-(Si(CH_3)_2)_3-C\equiv CH$.[85] $Cl(Si(CH_3)_2)_3Cl$ (15.1 g, 61.5 mmol) and 260 mL of 0.5 M HCCMgBr (129 mmol) gave 7.3 g (53%) of pure $HC\equiv C-(Si(CH_3)_2)_3-C\equiv CH$. Bp (30 mbar): 101 °C. ^1H NMR (200 MHz, C_6D_6): δ 2.16 (s, 2H, HC≡), 0.29 (s, 12H, $\equiv C-Si(CH_3)_2-$), 0.27 (s, 6H, $Si-Si(CH_3)_2-Si$). ^{29}Si NMR (59.62 MHz, pentane/D_2O): δ −33.6 ($\equiv C-Si(CH_3)_2-$), −47.1 ($Si-Si(CH_3)_2-Si$). MS (70 eV) *m/z* (rel. int.): 224 (M^+, 0.9).

$HC\equiv C-(Si(CH_3)_2)_4-C\equiv CH$. $Cl(Si(CH_3)_2)_4Cl$ (15.1 g, 49.7 mmol) and 210 mL of 0.5 M HCCMgBr (105 mmol) gave 9.2 g (65%) of pure $HC\equiv C-(Si(CH_3)_2)_4-C\equiv CH$. Bp (1 mbar): 90 °C. Anal. Calcd for $C_{12}H_{26}Si_4$: C, 50.99; H, 9.27. Found: C, 50.84; H, 9.16. ^1H NMR (200 MHz, C_6D_6): δ 2.18 (s, 2H, HC≡), 0.29 (s, 12H, $\equiv C-Si(CH_3)_2-$), 0.27 (s, 12H, $Si-Si(CH_3)_2-Si$). ^{13}C NMR (50.3 MHz, C_6D_6): δ 96.3, 88.9 (*C*≡C); −2.0, −5.9 ($Si(CH_3)_2$). ^{29}Si NMR (59.62 MHz, pentane/D_2O): δ −35.9 ($\equiv C-Si(CH_3)_2-$), −46.7 ($Si-Si(CH_3)_2-Si$). MS (70 eV) *m/z* (rel. int.): 282 (M^+, 0.9).

Cp*(dppe)Fe−C≡C−$(Si(CH_3)_2)_2$−C≡C−Fe(dppe)Cp* (1). This and the two following syntheses consist of two steps carried out in a one-pot fashion. A Schlenk tube was loaded with 0.740 g (1.0 mmol) of Cp*(dppe)FeOTf, 30 mL of diethyl ether, and a magnetic stirbar. Next, 98 μL of $HC\equiv C-(Si(CH_3)_2)_2-C\equiv CH$ was added by syringe. The reaction mixture was stirred overnight, during which time the initially green suspension turned progressively yellow. After decantation, the solid material was filtered by cannula and washed with 30 mL of pentane. Vacuum drying yielded the bis(vinylidene) derivative $[Cp^*(dppe)Fe=C=CH-(Si(CH_3)_2)_2-HC=C=Fe(dppe)Cp^*][OTf]_2$ (**13**) as an ocre solid (0.770 g, 96%), which was partially characterized before being converted into the bis(ethynediyl)disilane bis(organoiron) complex **1** of interest. FT-IR (KBr, cm^{-1}): 1606 ν(C=C). ^1H NMR (200 MHz, acetone-d_6): δ 7.68−7.28 (m, 40H, Ph), 3.46 (s, 2H, =CH), 3.06 (m, 4H, CH_2), 2.72 (m, 4H, CH_2), 1.61 (s, 30H, C_5Me_5), −0.11 (s, 12H, $Si(CH_3)$). ^{13}C NMR (50.3 MHz, acetone-d_6): δ 342.2 (t, $^2J_{C-P}$ = 30 Hz, Fe=C), 135.4−129.3 (m, Ph), 101.6 (d, $^1J_{C-H}$ = 166 Hz, =CH), 98.2 (s, C_5Me_5), 30.0 (tt, $^1J_{C-H}$ = 129 Hz, CH_2), 9.9 (q, $^1J_{C-H}$ = 128 Hz, C_5Me_5), −1.3 (q, $^1J_{C-H}$ = 121 Hz, $Si(CH_3)$). ^{31}P NMR (81 MHz, acetone-d_6): δ 90.9 (s, dppe). To the Schlenk tube containing 0.510 g (0.310 mmol) of the above-prepared bis(vinylidene) complex **13** were added 30 mL of diethyl ether and 0.070 g (0.62 mmol) of potassium *tert*-butoxide. The reaction mixture was stirred overnight, providing an orange solution. The solvent was then removed under reduced pressure and the residue extracted with 30 mL of toluene. The toluene was evaporated to dryness, and the solid residue was washed with 2 × 30 mL of pentane before being dried in vacuo. Yield: 0.330 g (0.24 mmol, 80%) of an orange powder. Slow diffusion of pentane into a saturated toluene solution of **1** afforded orange crystals suitable for X-ray structure analysis. Anal. Calcd for $C_{80}H_{90}Fe_2P_4Si_2$: C, 71.53; H, 6.75. Found: C 71.74; H, 6.63. FT-IR (KBr, cm^{-1}): 1975 ν(C≡C). ^1H NMR (200 MHz, C_6D_6): δ 8.28−7.06 (m, 40H, Ph), 3.08 (m, 4H, CH_2), 2.07 (m, 4H, CH_2), 1.63 (s, 30H, C_5Me_5), 0.57 (s, 12H, $Si(CH_3)$). ^{13}C NMR (50.3 MHz, C_6D_6): δ 140.2−127.7 (m, Ph), 87.9 (s, C_5Me_5), 30.8 (tt, $^1J_{C-H}$ = 129 Hz, CH_2), 10.6 (q, $^1J_{C-H}$ = 128 Hz, C_5Me_5), 0.42 (q, $^1J_{C-H}$ = 121 Hz, $Si(CH_3)$). ^{31}P NMR (81 MHz, C_6D_6): δ 101.6 (s, dppe).

Cp*(dppe)Fe−C≡C−$(Si(CH_3)_2)_3$−C≡C−Fe(dppe)Cp* (2). In this case, the synthetic procedure was similar to that described above for the preparation of **1**. Cp*(dppe)FeOTf (3.18 g, 4.31 mmol) was reacted with 536 μL (2.15 mmol) of $HC\equiv C-(Si(CH_3)_2)_3-C\equiv CH$ in 60 mL of diethyl ether to provide, after washing with 2 × 30 mL of pentane and vacuum drying, 3.35 g (1.97 mmol, 91% yield) of the bis(vinylidene) derivative $[Cp^*(dppe)Fe=C=CH-(Si(CH_3)_2)_3-HC=C=Fe(dppe)Cp^*][OTf]_2$ (**14**) as a yellow powder that was partially characterized. FTIR (KBr, cm^{-1}): 1608 ν(C=C). ^1H NMR (200 MHz, acetone-d_6): δ 8.06−7.28 (m, 40H, Ph), 3.46 (s, 2H, =CH), 3.02 (m, 4H, CH_2), 2.73 (m, 4H, CH_2), 1.63 (s, 30H, C_5Me_5), 0.08 (s, 6H, $Si(CH_3)$), −0.11 (s, 12H, $Si(CH_3)$). ^{13}C NMR (50.3 MHz, acetone-d_6): δ 341.9 (t, $^2J_{C-H}$ = 30 Hz, Fe=C), 139.9−129.1 (m, Ph), 101.6 (d, $^1J_{C-H}$ = 166 Hz, *C*=*C*H), 98.5 (s, C_5Me_5), 29.6 (tt, $^1J_{C-H}$ = 129 Hz, CH_2), 10.0 (q, $^1J_{C-H}$ = 128 Hz, C_5Me_5), −0.1 (q, $^1J_{C-H}$ = 121 Hz, $Si(CH_3)$), −6.63 (q, $^1J_{C-H}$ = 121 Hz, $Si(CH_3)$). ^{31}P NMR (81 MHz, acetone-d_6): δ 90.8 (s, dppe). The bis(vinylidene) compound **14** (3.15 g, 1.85 mmol) was then treated with 0.41 g (3.70 mmol) of *t*-BuOK in 60 mL of diethyl ether to give, after workup, 1.97 g (1.40 mmol, 76% yield) of **2** as an orange powder. Anal. Calcd for $C_{82}H_{96}Fe_2P_4Si_3$: C, 70.27; H, 6.90. Found: C, 69.78; H, 6.77. FT-IR (KBr, cm^{-1}): 1968 ν(C=C). ^1H NMR (200 MHz, C_6D_6): δ 8.22−7.06 (m, 40H, Ph), 3.07 (m, 4H, CH_2), 2.08 (m, 4H, CH_2), 1.62 (s, 30H, C_5Me_5), 0.58 (s, 12H, $Si(CH_3)$), 0.52 (s, 6H, $Si(CH_3)$). ^{13}C NMR (50.3 MHz, C_6D_6): δ 140.7−127.7 (m, Ph), 87.9 (s, C_5Me_5), 30.8 (tt, $^1J_{C-H}$ = 129 Hz, CH_2), 10.6 (q, $^1J_{C-H}$ = 128 Hz, C_5Me_5), 1.5 (q, $^1J_{C-H}$ = 121 Hz, $Si(CH_3)$), −5.0 (q, $^1J_{C-H}$ = 121 Hz, $Si(CH_3)$). ^{31}P NMR (81 MHz, C_6D_6): δ 101.5 (s, dppe).

Cp*(dppe)Fe−C≡C−$(Si(CH_3)_2)_4$−C≡C−Fe(dppe)Cp* (3). In this case, the synthetic procedure was also similar to that described above for the preparation of **1**. Cp*(dppe)FeOTf (1.52 g, 2.05 mmol) was reacted with 315 μL (1.0 mmol) of $HC\equiv C-(Si(CH_3)_2)_4-C\equiv CH$ in 60 mL of diethyl ether to provide 1.58 g (0.90 mmol, 90% yield) of the bis(vinylidene) derivative $[Cp^*(dppe)Fe=C=CH-(Si(CH_3)_2)_4-HC=C=Fe(dppe)Cp^*][OTf]_2$ (**15**) as a yellow powder that was partially characterized. FT-IR (KBr, cm^{-1}): 1619 ν(C=C). ^1H NMR (200 MHz, CD_2Cl_2): δ 7.83−7.55 (m, 40H, Ph), 3.30 (s, 2H, =CH), 2.96 (m, 4H, CH_2), 2.57 (m, 4H, CH_2), 1.57 (s, 30H, C_5Me_5), 0.05 (s, 12H, $Si(CH_3)_2$), −0.05 (s, 12H, $Si(CH_3)_2$). ^{13}C NMR (50.3 MHz, CD_2Cl_2): δ 341.9 (t, $^2J_{C-P}$ = 30 Hz, Fe=C), 139.3−116.9 (m, Ph), 103.2 (d, $^1J_{C-H}$ = 166 Hz, *C*=*C*H), 98.5 (s, C_5Me_5), 29.7 (tt, $^1J_{C-H}$ = 129 Hz, CH_2), 10.4 (q, $^1J_{C-H}$ = 128 Hz, C_5Me_5), 0.3 (q, $^1J_{C-H}$ = 121 Hz, $Si(CH_3)$), −5.5 (q, $^1J_{C-H}$ = 121 Hz, $Si(CH_3)$). ^{31}P NMR (81 MHz, CD_2Cl_2): δ 91.4 (s, dppe). The bis(vinylidene) complex **15** (1.36 g, 0.77 mmol) was then treated with 0.18 g (1.56 mmol) of *t*-BuOK in 60 mL of diethyl ether to give, after work up, 1.02 g (0.70 mmol, 91% yield) of **3** as

(81) Ishikawa, M.; Kumada, M.; Sakurai, H. *J. Organomet. Chem.* **1970**, *23*, 63–69.
(82) Gilman, H.; Inoue, S. *J. Org. Chem.* **1964**, *29*, 3418–3419.
(83) Connelly, N. G.; Geiger, W. E. *Chem. Rev.* **1996**, *96*, 877–910.
(84) Anders, U.; Krause, J. O.; Wang, D.; Nuyken, O.; Buchmeiser, M. R. *Des. Monomers Polym.* **2004**, *7*, 151–163.
(85) Ohshita, J.; Matsuguchi, A.; Furumori, K.; Hong, R. F.; Ishikawa, M.; Yamanaka, T.; Koike, T.; Shioya, J. *Macromolecules* **1992**, *25*, 2134–2140.

an orange powder. Slow diffusion of pentane into a saturated toluene solution of **3** afforded orange crystals suitable for X-ray structure analysis. Anal. Calcd for $C_{84}H_{102}Fe_2P_4Si_4$: C, 69.12; H, 7.04. Found: C, 69.37; H, 7.40. FT-IR (KBr, cm^{-1}): 1968 ν(C≡C). ^{1}H NMR (200 MHz, C_6D_6): δ 8.28−7.07 (m, 40H, Ph), 3.05 (m, 4H, CH_2), 2.02 (m, 4H, CH_2), 1.61 (s, 30H, C_5Me_5), 0.59 (s, 12H, $Si(CH_3)$), 0.51 (s, 12H, $Si(CH_3)$). ^{13}C NMR (50.3 MHz, C_6D_6): δ 165.8 (t, $^2J_{C-P}$ = 36 Hz, Fe−*C*≡C), 140.7−127.7 (m, Ph), 121.5 (s, Fe−C≡*C*), 87.9 (s, *C*$_5$Me$_5$), 31.2 (tt, $^1J_{C-H}$ = 129 Hz, CH_2), 10.6 (q, $^1J_{C-H}$ = 128 Hz, C_5*Me*$_5$), 1.7 (q, $^1J_{C-H}$ = 121 Hz, $Si(CH_3)$), −4.3 (q, $^1J_{C-H}$ = 121 Hz, $Si(CH_3)$). ^{31}P NMR (81 MHz, C_6D_6): δ 101.5 (s, dppe).

Isolation of the Bis[iron(III)] Derivatives [Cp*(dppe)Fe−C≡C−(Si(CH$_3$)$_2$)$_x$−C≡C−Fe(dppe)Cp*][BPh$_4$]$_2$ (1[BPh$_4$]$_2$−3[BPh$_4$]$_2$). A. 1[BPh$_4$]$_2$. To an orange slurry of **1** (0.41 g, 0.31 mmol) in CH_2Cl_2 (30 mL) cooled to −80 °C was added solid $[(C_5H_5)_2Fe][BPh_4]$ (0.31 g, 0.62 mmol). The stirred reaction mixture turned progressively dark-violet upon slow warming to −20 °C. At this temperature, the solution was filtered into a Schlenk tube containing pentane (80 mL) at −20 °C. A dark precipitate formed immediately. The solid residue was filtered off, washed with cold pentane, and dried under vacuum at low temperature to yield 0.71 g (0.35 mmol, 87%) of **1**[BPh_4]$_2$ as a dark-violet powder that is stable at −20 °C under an argon atmosphere. FT-IR (KBr, cm^{-1}): 1970 ν(C≡C). The CV data were identical to those of **1**.

B. 2[BPh$_4$]$_2$. This dark-violet compound, which is stable in the solid state at −20 °C under an argon atmosphere, was prepared and isolated following a procedure similar to that described above for **1**[BPh_4]$_2$, using 0.30 g (0.21 mmol) of **2** and 0.22 g (0.42 mmol) of $[(C_5H_5)_2Fe][BPh_4]$. Yield: 0.38 g (0.19 mmol, 90%). FT-IR (KBr, cm^{-1}): 1958 ν(C≡C). The CV data were identical to those of **2**.

C. 3[BPh$_4$]$_2$. To an orange slurry of **3** (0.17 g, 0.12 mmol) in CH_2Cl_2 (60 mL) cooled to −80 °C was added solid $[(C_5H_5)_2Fe][BPh_4]$ (0.10 g, 0.23 mmol). The reaction mixture was stirred overnight, during which time the temperature was allowed to slowly increase to 20 °C; the color turned progressively purple. The solvent was removed under reduced pressure and the solid residue quickly washed with pentane (2 × 30 mL) to yield 0.24 g (0.11 mmol, 97%) of **3**[BF_4]$_2$ as an air- and moisture-sensitive dark-violet powder, which can be stored at −20 °C. FT-IR (KBr, cm^{-1}): 1961 ν(C≡C). The CV data were identical to those of **3**. In a similar experiment, **3**[B(3,5-$(CF_3)_2C_6H_3)_4$]$_2$ was isolated upon oxidation of **3** with 2 equiv of Ag[B(3,5-$(CF_3)_2C_6H_3)_4$]. ESI MS (*m*/*z*) calcd for $C_{116}H_{114}F_{24}{}^{11}BSi_4P_4{}^{56}Fe_2$ ([M − {B(3,5-$(CF_3)_2C_6H_3)_4$}]$^+$): 2321.53568. Found: 2321.5433.

Chemical Reduction of 3[BPh$_4$]$_2$. To a cooled (−80 °C) purple THF solution (50 mL) of **3**[BPh_4]$_2$ (0.74 g, 0.35 mmol) was added solid cobaltocene (0.126 g, 0.67 mmol) under argon. The reaction mixture was stirred overnight, during which time the temperature was allowed to slowly increase to 20 °C; the color of the solution progressively changed from purple to orange. The solvent was removed under vacuum and the solid residue extracted with diethyl ether (8 × 50 mL). The extracts were combined and evaporated to dryness to yield 0.44 g (0.30 mmol, 86%) of **3** as an orange powder, identified by comparison of its FT-IR, CV, and NMR data with those of an authentic sample.

Electrochemical Experiments. All of the CV experiments were carried out at 20.0 ± 0.1 °C using a cell equipped with a jacket allowing circulation of water from the thermostat. The solvent was CH_2Cl_2 containing 0.1 M of *n*-Bu_4NPF_6 as the supporting electrolyte. The working electrode was a 1 mm diameter glassy carbon disk. It was carefully polished before each set of voltammograms with 1 μm diamond paste and ultrasonically rinsed in absolute ethanol. The electrochemical instrumentation consisted of a Tacussel GSTP4 programmer and a home-built potentiostat equipped with a positive-feedback compensation device.[86] The data were acquired with a Nicolet 310 oscilloscope. The counter electrode was a Pt wire and the reference electrode an aqueous SCE with a salt bridge containing the supporting electrolyte. The SCE electrode was checked against the ferrocene/ferrocenium couple (using the E° value of +0.460 V vs SCE in dichloromethane) before and after each experiment. Numerical simulations of the voltammograms were performed with the commercial BAS Digisim Simulator 3.1,[87] using the default numerical options with the assumption of planar diffusion. The Butler−Volmer law was considered for the electron-transfer kinetics.[88] The transfer coefficient, α, was taken as 0.5 with equal diffusion coefficients for all of the species ($D = 10^{-5}$ cm^2 s^{-1}).

Spectroelectrochemistry. UV−vis−NIR spectroelectrochemistry experiments were performed at 20 °C under argon with a homemade OTTLE cell (1 mm path length) using a Varian CARY 5000 spectrometer and an EG&G PAR model 362 potentiostat. A Pt mesh was used as the working electrode, a Pt wire as the counter electrode, and an Ag wire as a pseudoreference electrode. The electrodes were arranged in the cell such that the Pt mesh was in the optical path of the quartz cuvette. The anhydrous freeze−pump−thaw-degassed sample−electrolyte solution (0.1 M *n*-$Bu_4N^+OTf^-$) was cannula-transferred under argon into the cell, which had previously been thoroughly deoxygenated.

X-ray Crystal Structure Determinations. Single crystals of compounds **1** and **3**·$^2/_3C_7H_8$ suitable for X-ray structure determination were obtained as described above and mounted with epoxy cement on the tip of a glass fiber. Crystal data and data collection and refinement parameters are given in Table S2 in the Supporting Information.

Compound **1** was studied at 120(1) K on a Kappa-CCD Enraf-Nonius diffractometer, whereas compound **3**·$^2/_3C_7H_8$ was studied on an APEX II Bruker-AXS diffractometer at 100(2) K; both instruments were equipped with a bidimensional CCD detector employing graphite-monochromatized Mo Kα radiation (λ = 0.71073 Å). The two structures were solved with SIR-97, which revealed the non-hydrogen atoms.[89] After anisotropic refinement, the remaining atoms were found in Fourier difference maps. The complete structures were then refined with SHELXL97 by full-matrix least-squares procedures on reflection intensities (F^2).[90] The structure of **3** contains one independent toluene molecule that is ordered at low temperature and a very disordered solvent molecule that was not located precisely. The contribution of the disordered solvent to the calculated structure factors was estimated following the bypass algorithm[91] implemented in the SQUEEZE option in PLATON.[92] A new data set, free of solvent contributions, was then used in the final refinement. In both cases, the non-hydrogen atoms were refined with anisotropic displacement coefficients, and all of the hydrogen atoms were placed in idealized locations. Atomic scattering factors were taken from the literature.[93] Ortep views of **1** and **3**·$^2/_3C_7H_8$ were generated with PLATON-98.[94] Compounds **1** and **3**·$^2/_3C_7H_8$ were submitted to the Cambridge Crystallographic

(86) Garreau, D.; Savéant, J.-M. *J. Electroanal. Chem.* **1972**, *35*, 309–331.
(87) Rudolph, M.; Reddy, D. P.; Felberg, S. W. *Anal. Chem.* **1994**, *66*, 560A–589A.
(88) Bard, A. J.; Faulkner, L. R. *Electrochemical Methods: Fundamentals and Applications*, 2nd ed.; Wiley: New York, 2000.
(89) Altomare, A.; Burla, M. C.; Camali, M.; Cascarano, G.; Giacovazzo, C.; Guagliardi, A.; Moliterni, A. G. G.; Polidori, G.; Spagna, R. *J. Appl. Crystallogr.* **1999**, *31*, 115–119.
(90) Sheldrick, G. M. *SHELX97: A Program for Refinement of Crystal Structures*; University of Göttingen: Göttingen, Germany, 1997.
(91) Sluis, P. v. d.; Spek, A. L. *Acta Crystallogr.* **1990**, *A46*, 194–201.
(92) Spek, A. L. *Acta Crystallogr.* **1990**, *A46*, C34.
(93) *International Tables for X-ray Crystallography*; Wilson, A. J. C., Ed.; Kluwer Academic Publishers: Dordrecht, The Netherlands, 1992; Vol. C.
(94) Spek, A. L. *PLATON-98: A Multipurpose Crystallographic Tool*; Utrecht University: Utrecht, The Netherlands, 1998.

Data Centre (CCDC, http://www.ccdc.cam.ac.uk) under reference numbers 298794 and 221990, respectively.

Acknowledgment. Financial support from the Austrian−French scientific exchange program (AMADEUS 20/2004-05), the Centre National de la Recherche Scientifique (CNRS), the Technische Universität Graz, and the Université de Rennes 1 is gratefully acknowledged.

Supporting Information Available: Additional details of the reaction of **8** with HCC−$(Si(CH_3)_2)_x$−CCH, selected IR data for Fe(II) and Fe(III) acetylides (Table S1), crystallographic data collection and structure refinement parameters for **1** and **3** (Table S2), working curve for the determination of $\Delta E°$ (Figure S1), simulated and experimental cyclic voltammograms of **1**, **2**, and **3** (Figure S2), X-band EPR spectra of **1**[BPh_4], **1**[BPh_4]$_2$, and **2**[BPh_4]$_2$ (Figures S3−S5), temperature dependence of $\chi_M T$ for a powdered sample of **2**[BPh_4]$_2$ (Figure S6), and CIF files for the reported X-ray crystal structures of **1** and **3**·$^2/_3C_7H_8$. This material is available free of charge via the Internet at http://pubs.acs.org.

JA804608Z